

CRAFT: Time Series Forecasting with Cross-Future Behavior Awareness

Yingwei Zhang^{1,2,*}, Ke Bu^{3,*}, Zhuoran Zhuang³, Tao Xie^{1,2}, Yao Yu³, Dong Li³, Yang Guo^{1,2}, Detao Lv^{3,†}

¹Beijing Key Laboratory of Mobile Computing and Pervasive Device, Institute of Computing Technology, Chinese Academy of Sciences, Beijing, China

²University of Chinese Academy of Sciences, Beijing, China

³Alibaba Group

zhangyingwei@ict.ac.cn, {bk264304,detao.ldt}@alibaba-inc.com

Abstract

The past decades witness the significant advancements in time series forecasting (TSF) across various real-world domains, including e-commerce and disease spread prediction. However, TSF is usually constrained by the uncertainty dilemma of predicting future data with limited past observations. To settle this question, we explore the use of Cross-Future Behavior (CFB) in TSF, which occurs before the current time but takes effect in the future. We leverage CFB features and propose the **C**ross-Future Behavior Awareness based **T**ime Series Forecasting method (CRAFT). The core idea of CRAFT is to utilize the trend of cross-future behavior to mine the trend of time series data to be predicted. Specifically, to settle the sparse and partial flaws of cross-future behavior, CRAFT employs the Koopman Predictor Module to extract the key trend and the Internal Trend Mining Module to supplement the unknown area of the cross-future behavior matrix. Then, we introduce the External Trend Guide Module with a hierarchical structure to acquire more representative trends from higher levels. Finally, we apply the demand-constrained loss to calibrate the distribution deviation of prediction results. We conduct experiments on real-world dataset. Experiments on both offline large-scale dataset and online A/B test demonstrate the effectiveness of CRAFT. Our dataset and code are available at <https://github.com/CRAFTinTSF/CRAFT>.

1 Introduction

Time series forecasting (TSF) is the crucial infrastructure of various real-world domains, including e-commerce [Wen *et al.*, 2017], traffic [Hu *et al.*, 2024], disease spread prediction [Mossop and Rahman, 2023], and stock price prediction [Shetty and Ismail, 2023].

However, accurate TSF is a challenging task given the need to model complex, non-linear temporal patterns over long periods of time [Rasul *et al.*, 2024]. To this end, researchers explore various backbone networks such as convolutional neural networks (CNNs) [Chen *et al.*, 2020], recurrent neural networks (RNNs) [Yin *et al.*, 2022], and

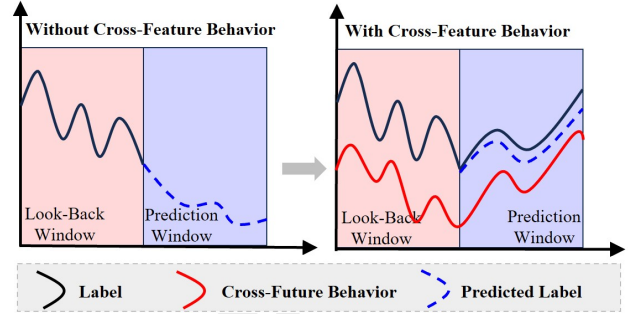


Figure 1: Illustration of Cross-Future Behavior (CFB).

Transformer [Zhou *et al.*, 2021]. Additionally, they work on incorporating richer features into TSF and study issues related to multivariate TSF [Zhao and Shen, 2024; Li *et al.*, 2024] and feature decomposition [Zeng *et al.*, 2023; Liu *et al.*, 2024b]. With the advancement of sensing technology, such as Internet data in e-commerce and population mobility information in disease spread prediction, various priori information for TSF can be recorded. In this paper, we defined these priori information as **Cross-Future Behavior (CFB)**: features that occur before the current time but take effect in the future. CFB positively affects TSF. As shown in Figure 1, if only relying on the trend of the label, the future trend may be predicted as a downward trend. With the guidance of CFB, the prediction result will be more precise.

In fact, existing work is also attempting to introduce more features into TSF. [Zeng *et al.*, 2023] attempts to extract more information from the acquired data and decomposes the time series into trend and remainder parts. [Wen *et al.*, 2017] classifies covariate features in TSF into dynamic historical, known future, and static variables. CFB, we proposed in this paper, can be treated as the known future variable and has many excellent properties. CFB contains true information related to future events. The future trend of the prediction target, even the abnormal trend caused by sudden events, can be reflected in the trend of CFB. However, as the existing TSF models primarily focus on exploring the correlation between the historical series and future trends [Chen *et al.*, 2020; Yin *et al.*, 2022; Zhou *et al.*, 2021], it is difficult to achieve TSF that integrates CFB through existing models. Taking the e-commerce scenario as an example, CFB-based TSF faces two main challenges. **1) CFB is sparse and partial.** Con-

sumers can book items at any time, causing CFB to remain fully observed until the last minute. Thus, if CFB is simply incorporated into the model, the prediction model may be unable to apply CFB features correctly and even make incorrect predictions due to CFB. **2) The trend of CFB is unobvious.** Compared with the sales trend in a business district, the sales trend in an individual hotel is unobvious. CFB has the same nature, and the trend in an individual hotel is much unobvious compared with that in a high-level business district. Consequently, devising a method to utilize the sales trend in high level to inform the auxiliary forecast for an individual hotel presents another significant challenge.

Therefore, jointly considering the above challenges, we propose CRAFT, a **Cross-Future Behavior Awareness based Time Series Forecasting** method, for the first time to utilize Cross-Future Behavior to realize time series forecasting. The core idea of CRAFT, as shown in Figure 1, is to utilize the trend of CFB to mine the trend of time series data to be predicted. CRAFT is composed of three main parts: the Koopman Predictor Module (KPM), the Internal Trend Mining Module (ITM), and the External Trend Guide Module (ETG). KPM can extract the key trends of the label and CFB, predicting the label in the prediction window. ITM supplements the unknown area of CFB, making the final prediction of the label in the prediction window. ETG, with a hierarchical structure, can acquire more representative trends from higher levels. Finally, we apply the demand-constrained loss to calibrate the distribution deviation of prediction results. We conduct experiments on real-world dataset. Experiments on both offline large-scale dataset and online A/B test demonstrate the effectiveness of CRAFT. We summarize the main contributions of this paper as follows:

- We define CFB and apply CFB to TSF for the first time. CFB is a feature discovered from our extensive real case studies and has superior characteristics: the trend of CFB can reflect the prediction target and even the abnormal trend of the target.
- We propose a novel framework, namely CRAFT, to realize CFB-based time series forecasting. CRAFT can utilize the trend of CFB to mine the trend of prediction targets. CRAFT is composed of three main modules, including KPM, ITM, and ETG. KPM and ITM can address the sparse and partial flaws of CFB, and ETG can address the unobvious trend flaws of CFB.
- Extensive offline experiments on the real-world dataset and online A/B tests show the superiority of CRAFT towards SOTA baselines. CRAFT improves application performance significantly, with an improvement rate of 41.35% on the *IWR* metric. Currently, CRAFT has been successfully deployed on the reality application.

2 Related Work

Backbone for time series forecasting. Recently, Transformer has reshaped the landscape of TSF across numerous fields [Wen *et al.*, 2023]. PatchTST [Nie *et al.*, 2024] designs a channel-independent Transformer for time series forecasting. To address the channel-independent limitations of Transformer, CARD [Wang *et al.*, 2024] proposes a

channel-aligned attention structure that can acquire both temporal correlations and dynamical dependence among multiple variables over time. Informer [Zhou *et al.*, 2021] extends Transformer using ProbSparse based on KL divergence to solve Long Sequence time series forecasting. TFT [Lim *et al.*, 2021] introduces a novel attention-based architecture that combines high-performance multi-horizon forecasting with interpretable insights into temporal dynamics. Autoformer [Wu *et al.*, 2021] proposes a Decomposition Architecture and Auto-Correlation Mechanism based on stochastic process theory to realize the series-wise connection and break the bottleneck of information utilization. Pyraformer [Liu *et al.*, 2021] proposes a new Transformer based on a pyramidal attention module to simultaneously capture temporal dependencies of different ranges in a compact multi-resolution fashion. Besides Transformer, a variety of other network architectures are widely investigated. CNNs-based time series forecasting models such as WaveNet [Oord *et al.*, 2016], TCN [Bai *et al.*, 1803], and DeepTCN [Chen *et al.*, 2020] use causal convolution to learn sequences and use dilated convolution and residual block to memorize historical patterns. Graph WaveNet [Zonghan *et al.*, 2019] enhances the WaveNet framework by using an adaptive and learnable adjacency matrix to automatically infer graph structures, enabling the prediction of spatiotemporal sequences. Moreover, due to the sequential nature of time series data, RNNs-based time series forecasting is particularly widely suited, mainly modeling the temporal dependence of time series [Salinas *et al.*, 2020; Wang *et al.*, 2019; Liu *et al.*, 2020].

Multivariate time series forecasting. Multivariate TSF utilizes multiple time-dependent variables to realize prediction. Compared with univariate TSF, multivariate TSF can understand the interactions between different components of a complex system better, which is crucial for strategy formulation and decision-making [Mendis *et al.*, 2024]. There are two commonly used strategies in multivariate TSF, i.e., the channel-dependent (CD) and channel-independent (CI) methods. CI method only models cross-time dependence, and the CD method models both cross-time dependence and cross-variate dependence [Zhao and Shen, 2024; Yang *et al.*, 2024]. While the CI method is characterized by simplicity and low risk of overfitting, the CD method has inevitably become the mainstream of research. Recently, [Zhao and Shen, 2024] utilizes the channel dependence between variates and proposes a plug-and-play method named LIFT, which exploits the lead-lag relationship between variates by estimating leading indicators and leading steps, refreshing multivariate TSF’s performance.

Feature decomposition in time series forecasting. Different from multivariate TSF utilizing multiple variates and the dependence between variates to realize prediction, feature decomposition in TSF does not introduce new variates. The core idea of feature decomposition is to extract as much information as possible from existing variates. Dlinear [Zeng *et al.*, 2023] decomposes time series into trend series and remainder series and uses two single-layer linear networks to model them, bringing performance improvements. Koopa [Liu *et al.*, 2024b] solves non-stationary time series

prediction problems from the perspective of modern dynamics Koopman theory.

3 Preliminaries

Time series forecasting (TSF) with Cross-Future Behavior (CFB) can be defined as $\mathbf{Y}_{t+1:t+P} = H(\mathbf{Y}_{t-L+1:t}, \mathbf{X}_T, \mathbf{C}_T)$. $\mathbf{Y}_{t-L+1:t} \in \mathbb{R}^L$ and $\mathbf{Y}_{t+1:t+P} \in \mathbb{R}^P$ are time series data (i.e., label) at the L -length look-back window and P -length prediction window at time t respectively. \mathbf{X}_T is covariate features, \mathbf{C}_T is the CFB feature and H is the prediction function to be learned. The covariate features [Wen *et al.*, 2017] \mathbf{X}_T contains three categories: 1) historical features like month-on-month sales features, etc; 2) known future features like holidays, weekends, etc; 3) static features like hotel brands, business districts, etc. $\mathbf{C}_T = \{\mathbf{C}_{t-L+1:t}, \mathbf{C}_{t+1:t+P}\}$, where $\mathbf{C}_{t-L+1:t}$ is CFB in the look-back window and $\mathbf{C}_{t+1:t+P}$ is CFB in the prediction window. It is worth noting that $\mathbf{C}_{t+1:t+P}$ in the prediction window is partial as this is a not fully observable variate. Consumers can book items in the prediction window at any time until the last minute. More detailed introduction to CFB feature \mathbf{C}_t refers to Appendix A in our full paper [Zhang *et al.*, 2025].

In the following section, we omit the subscripts of some symbols for simplicity. Specifically, we denote time series at the look-back window $\mathbf{Y}_{t-L+1:t}$ as \mathbf{Y}_L , time series at the prediction window $\mathbf{Y}_{t+1:t+P}$ as \mathbf{Y}_P , CFB feature in look-back window $\mathbf{C}_{t-L+1:t}$ as \mathbf{C}_L , CFB feature in prediction window $\mathbf{C}_{t+1:t+P}$ as \mathbf{C}_P . In addition, as \mathbf{C}_P is partial observed, we define a new notion \mathbf{C}_{TP} to indicate the ground truth of CFB in prediction window.

4 Methodology

Figure 2 depicts the overview of the proposed CRAFT method. CRAFT uses DLinear [Zeng *et al.*, 2023] to decompose the time series data $\mathbf{Y}_L, \mathbf{C}_L$ in the look-back window into the trend $\mathbf{Y}_L^T, \mathbf{C}_L^T$ and residual $\mathbf{Y}_L^R = \mathbf{Y}_L - \mathbf{Y}_L^T, \mathbf{C}_L^R = \mathbf{C}_L - \mathbf{C}_L^T$ components. The moving average kernel with a certain kernel size is used in the decomposition process. CRAFT’s core idea lies in how to use the trend of partial CFB to mine the trend of label. We prove the consistency between partial CFB, CFB, and label theoretically in Appendix D.1 and D.2 in our full paper [Zhang *et al.*, 2025]. CRAFT is composed of three submodules: Koopman Predictor Module (KPM), Internal Trend Mining Module (ITM), and External Trend Guide Module (ETG). KPM employs the Koopman operator to linearly map the CFB features from the look-back window to the prediction window, after projecting the raw data into the mapping space. Subsequently, it supervises the initialization of the label sequence within the prediction window. ITM completes linear mapping between the look-back window and prediction window and adopts an adaptation operator to instruct the evolution of the time series of the label sequentially. Due to higher-level temporal sequences having lower noise and stronger regularity compared to lower-level temporal sequences, ETG module makes forecast results more robust by structuring the reconciliation matrix and calibrating the predicted outcomes of root nodes. To avoid

computational problems caused by excessively large hierarchical matrices, the concept of hierarchical sampling is introduced.

4.1 Koopman Predictor Module

KPM module aims to transfer the future trend information from CFB feature $\mathbf{C}_T = \{\mathbf{C}_L, \mathbf{C}_P\}$ to labels \mathbf{Y}_P . The simplified framework of KPM is shown in Figure 2 and the specific framework refers to Appendix C.1 in our full paper [Zhang *et al.*, 2025]. KPM employs an encoder-decoder framework with the input of CFB \mathbf{C}_L and label \mathbf{Y}_L in the look-back window and output of partial CFB \mathbf{C}_P in the prediction window. Concretely, we first construct an encoder $\mathbb{R}^L \mapsto \mathbb{R}^D$ as a data-driven measurement function. The encoder module is Multi Layer Perception (MLP) [Zhu *et al.*, 2023] and it can also be replaced to other structure: $\mathbf{ZC}_L^T = \text{Encoder}(\mathbf{C}_L^T), \mathbf{ZC}_P = \text{Encoder}(\mathbf{C}_P), \mathbf{ZY}_L^T = \text{Encoder}(\mathbf{Y}_L^T)$, where $\mathbf{ZC}_L^T, \mathbf{ZC}_P, \mathbf{ZY}_L^T$ are the embeddings of the trend of CFB in the look-back window, CFB in the prediction window, and the trend of labels in the look-back window. In particular, the encoder is shared for $\mathbf{ZC}_L^T, \mathbf{ZC}_P, \mathbf{ZY}_L^T$. Secondly, based on the Koopman Theory [Koopman, 1931], we use finite linear matrix \mathbf{K}_C to approach infinite koopman matrix \mathcal{K} to simulate the evolution process between time periods, that is:

$$\hat{\mathbf{ZC}}_P = \mathbf{K}_C \times \mathbf{ZC}_L^T, \quad (1)$$

where $\mathbf{K}_C \in \mathbb{R}^{D \times D}$ is the Koopman matrix for CFB, which contains the future sales trend information. Its value can be approximated by ridge regression as:

$$\mathbf{K}_C = (\mathbf{ZC}_L^{T^T} \times \mathbf{ZC}_L^T + \lambda \mathbf{E})^{-1} \times \mathbf{ZC}_L^{T^T} \times \hat{\mathbf{ZC}}_P. \quad (2)$$

Then, we use \mathbf{K}_C to convert the future trend information from CFB embedding to label embedding:

$$\hat{\mathbf{ZY}}_{Init}^T = \mathbf{K}_C \times \mathbf{ZY}_L^T. \quad (3)$$

Finally, we construct a decoder $\mathbb{R}^D \mapsto \mathbb{R}^P$ to obtain the preliminary prediction result of label. Same as encoder, decoder can adopt various model structures, and this paper uses the MLP layer [Zhu *et al.*, 2023]. In particular, the decoder is shared for $\hat{\mathbf{C}}_P, \hat{\mathbf{Y}}_{Init}^T$: $\hat{\mathbf{C}}_P = \text{Decoder}(\hat{\mathbf{ZC}}_P), \hat{\mathbf{Y}}_{Init}^T = \text{Decoder}(\hat{\mathbf{ZY}}_{Init}^T)$. Specifically, to ensure that \mathbf{K}_C is meaningful, we construct a recovery loss $\mathcal{L}_{be,k}$ to constrain the decoder to restore the original data based on the embedding output by the encoder, so that the embedded latent variable enables to obtain the potential attributes from raw data and preserve the original information as much as possible. $\mathcal{L}_{be,k}$ is designed based on the MSE loss:

$$\mathcal{L}_{be,k} = \frac{2}{P^2} \sum_{i=0}^P \sum_{j=0}^i (\hat{\mathbf{C}}_P[i, j] - \mathbf{C}_P[i, j])^2, \quad (4)$$

we choose \mathbf{C}_P to calculate loss because we emphasize more on tendency characterization at the prediction window. It should be noted that we only focus on the known parts, i.e., $j \leq i$, and the loss of the masked data will not be calculated.

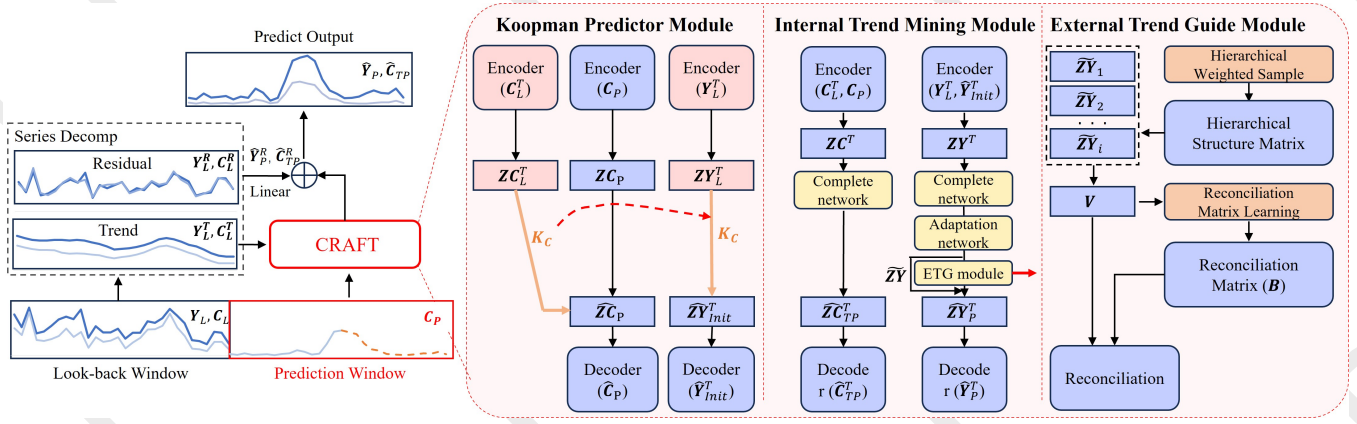


Figure 2: The overview of the proposed Cross-Future Behavior Awareness based Time Series Forecasting method (CRAFT). The left decomposition part is based on DLinear. CRAFT is composed of three main parts, the Koopman Predictor Module (KPM), the Internal Trend Mining Module (ITM), and the External Trend Guide Module (ETG). KPM is used to extract the key trends of the trend of label and CFB, predicting the label in the prediction window. ITM is used to supplement the unknown area of the CFB. ETG is used to acquire more representative trends from higher levels.

4.2 Internal Trend Mining Module

ITM module aims to complete the CFB feature. After KPM, we attained preliminary insufficient prediction $\hat{\mathbf{Y}}_{init}^T$. In the ITM module, we first adopt a complete network to patch the mapping of CFB from the look-back window to the prediction window and then employ an adaptation network to fulfill the adaptive migration of data distribution from CFB to the label. The simplified framework is in Figure 2 and the specific framework is in Appendix C.2 in our full paper [Zhang *et al.*, 2025]. We utilize another pair of encoder $\mathbb{R}^{L+P} \mapsto \mathbb{R}^D$ and decoder $\mathbb{R}^D \mapsto \mathbb{R}^{L+P}$ to learn the common embedding for entire known information. Unlike KPM, ITM takes all known information as input, i.e., data in the train and prediction window. Regarding the label, we pad preliminary predicted values $\hat{\mathbf{Y}}_{init}^T$ at the prediction window: $\mathbf{ZC}^T = \text{Encoder}(\text{concat}(\mathbf{C}_L^T, \mathbf{C}_P))$, $\mathbf{ZY}^T = \text{Encoder}(\text{concat}(\mathbf{Y}_L^T, \hat{\mathbf{Y}}_{init}^T))$. To settle the forecast window puzzle, we use the complete network to extend known curves into unknown regions, which is designed as a linear network:

$$\hat{\mathbf{ZC}}_{TP}^T = \text{Complete_network}(\mathbf{ZC}^T). \quad (5)$$

Additionally, despite there being a certain correlation between CFB and label, their distributions are not entirely identical. Based on this fact, we employ an adaptation network to adjust the label adaptively, with the ETG module (4.3) following closely behind. Since both the complete network and adaptation network operate on the hidden variable \mathbf{ZY}^T based on the original attributes of labels, we merge them into the ITM module to distinguish it from the ETG module. After traversing from the ITM & ETG module, we acquire the desired latent variable $\hat{\mathbf{ZY}}_P^T$:

$$\begin{aligned} \tilde{\mathbf{ZY}} &= \text{Adaptation_network}(\text{Complete_network}(\mathbf{ZY}^T)), \\ \hat{\mathbf{ZY}}_P^T &= \text{ETG_module}(\tilde{\mathbf{ZY}}). \end{aligned} \quad (6)$$

Finally, the latent vector $\hat{\mathbf{ZC}}_{TP}^T$ and $\hat{\mathbf{ZY}}_P^T$ are converted into target predicted values with decoder: $\hat{\mathbf{C}}_{TP}^T = \text{Decoder}(\hat{\mathbf{ZC}}_{TP}^T)$, $\hat{\mathbf{Y}}_P^T = \text{Decoder}(\hat{\mathbf{ZY}}_P^T)$.

The final result is calculated by adding these two values with the reminder predicted values (acquired with the linear mapping of $\mathbf{Y}_L^R, \mathbf{C}_L^R$ in Figure 2, $\hat{\mathbf{C}}_{TP}^R = \text{Linear}(\mathbf{C}_L^R)$, $\hat{\mathbf{Y}}_P^R = \text{Linear}(\mathbf{Y}_L^R)$):

$$\hat{\mathbf{C}}_{TP} = \hat{\mathbf{C}}_{TP}^T + \hat{\mathbf{C}}_{TP}^R, \quad \hat{\mathbf{Y}}_P = \hat{\mathbf{Y}}_P^T + \hat{\mathbf{Y}}_P^R. \quad (7)$$

To ensure the effectiveness of complete network, we introduce the prediction bias loss \mathcal{L}_{be-y} :

$$\mathcal{L}_{be-y} = \frac{2}{k^2} \sum_{i=0}^k \sum_{j=0}^k (\hat{\mathbf{C}}_{TP}[i, j] - \mathbf{C}_{TP}[i, j])^2. \quad (8)$$

4.3 External Trend Guide Module

ETG module is designed to settle the trend unobvious challenge, which uses aggregated spatial dimension to improve prediction results. Aggregated spatial dimension has stronger regularity, less noise, and is easier to estimate. Table 1 shows that the sample size of the hotel is approximately $400k$, which is too extensive for direct model train. Therefore, referring to [Lu *et al.*, 2022], we introduced a hierarchical sampling strategy to construct samples. This strategy assumes the global reconciliation matrix \mathbf{P} is sparse, indicating that only child nodes belonging to the same parent node have calibration relationships with each other. This assumption aligns well with the geographic attributes of hotels. We aggregate hotels into business districts based on their geographic location and then to higher levels of urban granularity. First, we randomly pick a business district. Then, we sample m hotels from this district, with the likelihood of selection increasing with each hotel’s historical label value. These m hotels’ labels are combined to create a virtual parent node. Together, the $m + 1$ nodes form a sampled hierarchy that serves as model input. This hierarchical sampling maintains the sum constraint through virtual parent nodes, and label weighted

sampling aligns the virtual sequence more with the real parent sequence. Moreover, these strategies reduce the reconciliation matrix's parameter count from $\mathcal{O}(n^2)$ to $\mathcal{O}(mn)$, significantly easing the model's computational load.

The framework of ETG is detailed in Figure 2 and Appendix C.3 in our full paper [Zhang *et al.*, 2025]. The input of ETG is $\tilde{\mathbf{Z}}\mathbf{Y}$ (Eq. (6)). $z_{i/j/k} = \tilde{\mathbf{Z}}\mathbf{Y}[i/j/k]$ are the elements of $\tilde{\mathbf{Z}}\mathbf{Y}$. According to the hierarchical sampling, we can adjust its shape from $[Bt, \dots]$ to $[g, m, \dots]$, where $Bt = g \times m$, indicating the number of original nodes, the number of nodes in high-level and in low-level. All subsequent actions are operated within the virtual hierarchical group. We obtain the key and query to calculate the reconciliation matrix \mathbf{B} between nodes in the same hierarchical structure, where $\mathbf{B}(i, j)$ indicates the reconciliation relationship between the i th and j th nodes in the hierarchical structure:

$$e_{ij} = \mathbf{W}_q z_i \odot \mathbf{W}_k z_j, \mathbf{B}[i, j] = \frac{\exp(e_{ij})}{\sum_{k \in \mathcal{M}_i} \exp(e_{ik})}, \quad (9)$$

where $\mathbf{W}_q \in \mathbb{R}^{d \times d}$, $\mathbf{W}_k \in \mathbb{R}^{d \times d}$ are the query and key parameter of model, \mathcal{M}_i is the set of nodes in the current hierarchy of i . Then, we use the reconciliation matrix \mathbf{B} to calibrate each sequence:

$$\hat{z}_i = \sum_{k \in \mathcal{M}_i} \mathbf{B}[i, k] \times \mathbf{W}_v \times z_k, \quad (10)$$

where $\mathbf{W}_v \in \mathbb{R}^{d \times d}$ is the model's value parameter. Given the lower noise and greater regularity of parent nodes compared to child nodes, we refrain from applying representation calibration to parent nodes using masking techniques, aligning with the reconciliation process. During the model training process, we introduce reconciliation loss to implement hierarchical constraints:

$$\mathcal{L}_{recon} = \frac{1}{g^2} \sum_{i=0}^g (\hat{\mathbf{Y}}_P[i^H] - \sum_{j=0}^m \hat{\mathbf{Y}}_P[i, j])^2. \quad (11)$$

where $\hat{\mathbf{Y}}_P[i^H]$ is the estimated result of parent node. \mathcal{L}_{recon} indicates the difference between the direct estimation of the parent node and sum of underlying estimation results, ensuring the sum of the calibrated estimated results of the underlying nodes approach parent node's estimated results.

4.4 Algorithm Inference

To fully utilize demand information related to cross-future behavior, we constructed the demand-constrained loss. In practice, we have found that there are invisible boundaries on the amount of user demand. Inspired by [Avati *et al.*, 2020; Gao *et al.*, 2022], we are conscious that the boundary is informative for the model. Thus, we construct upper and lower limits based on the demand in transaction scenarios and design a demand-constrained loss to digest this boundary information. The principle is shown in Figure 3. From the perspective of likelihood estimation, we make assumptions about the distribution of labels when using the common MAE or MSE as a loss function. Taking the MSE loss function used in this paper as an example, the MSE loss function is based on the assumption that the predicted target follows a Gaussian distribution, and what our model infers is the mean of

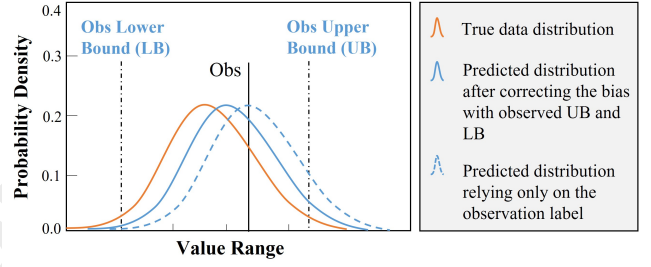


Figure 3: Demand-Constrained Loss.

the Gaussian distribution. The actual observation may not necessarily be the mean of true Gaussian distribution. With the assistance of upper and lower limits, we can support the model hover the true distribution.

In the check-in scenario of the hotel, we regard the truth value as label y (i.e., \mathbf{Y}) and regard the value for the day of reservation as the lower demand bounds y_l , excluding entire CFB actions. We also consider the page view of the order page as the upper bound y_u , including the unconverted potential user data. The demand-constrained loss is as follows:

$$f_d(\hat{y}, y, y_l, y_u) = \begin{cases} (\hat{y} - y)^2 + \beta(\hat{y} - y_l)^2, & \hat{y} < y_l \\ (\hat{y} - y)^2, & y_l \leq \hat{y} \leq y_u \\ (\hat{y} - y)^2 + \beta(\hat{y} - y_u)^2, & \hat{y}_u < \hat{y}, \end{cases} \quad (12)$$

where β is hyperparameter. We define the main loss as \mathcal{L}_y , indicating the forecast bias of \mathbf{Y}_P :

$$\mathcal{L}_y = f_d(\hat{\mathbf{Y}}_P, \mathbf{Y}_P, \mathbf{Y}_P^L, \mathbf{Y}_P^U). \quad (13)$$

where \mathbf{Y}_P^L is the lower bound matrix, and \mathbf{Y}_P^U is the upper bound matrix. Through the aforementioned submodules, CRAFT enables the future trend of cross-future behavior to approach consummation and migrate it to the tendency cognition of label, aggregating to higher-level label to perceive more distinct and precise inclination subsequently. During the process, we obtain $\hat{\mathbf{C}}_P$ which is transferred from encoder to decoder to constrain the representation of koopman embedding, the intact matrix expression of prediction window of cross-future behavior $\hat{\mathbf{C}}_{TP}$, and ultimate desired prediction results $\hat{\mathbf{Y}}_P$. To achieve better model outcome, the loss of CRAFT consists of four parts, where $\alpha_n, n \in 1, 2, 3$ are hyper parameters used to balance multiple losses:

$$\mathcal{L} = \mathcal{L}_y + \alpha_1 \mathcal{L}_{be,k} + \alpha_2 \mathcal{L}_{be,y} + \alpha_3 \mathcal{L}_{recon}. \quad (14)$$

$\mathcal{L}_{be,k}$, $\mathcal{L}_{be,y}$, \mathcal{L}_{recon} , \mathcal{L}_y are shown in Eq. (4), Eq. (8), Eq. (11), and Eq. (12) which corresponding to the recovery loss of $\hat{\mathbf{C}}_P$ in the KPM module, the prediction error of $\hat{\mathbf{C}}_{TP}$ in the ITM module, the reconstruction drift of $\hat{\mathbf{Y}}_P$ at the ETG module and the forecast deviation of label $\hat{\mathbf{Y}}_P$ respectively.

5 Experiments

5.1 Experimental Settings

Dataset

We conduct offline experiments on real-world dataset collected in May 2023 at Fliggy. To reflect the model effects

Hierarchy	# of city	# of business	# of hotel
Volume	0.4k	5k	400k

Table 1: Dataset Statistics.

on different data distributions objectively, the prediction window we cover to verify the model’s effectiveness contains both holidays and daily events. In addition, we set different forecast lengths $K \in \{7, 14, 30\}$, corresponding to look-back lengths $T \in \{30, 90, 180\}$. The dataset statistics are shown in Table 1. The hotels we use for verification are located in over 400 cities, covering more than 5000 business districts. The total sample size is around 400k.

Baseline Methods and Evaluation Metrics

The baseline methods for comparison include MQ-RNN [Wen *et al.*, 2017], Informer [Zhou *et al.*, 2021], DLinear [Zeng *et al.*, 2023], Koopa [Liu *et al.*, 2024b], TFT [Lim *et al.*, 2021], Autoformer [Wu *et al.*, 2021], Fedformer [Zhou *et al.*, 2022] and iTransformer [Liu *et al.*, 2024a].

Weighted Mean Absolute Percentage Error ($wMAPE$) is adopted to measure the models’ performance in offline experiments:

$$wMAPE = \frac{\sum |y - \hat{y}|}{\sum y}, \quad (15)$$

where y denotes the ground truth and \hat{y} denotes the predicted value. In hotel booking situations, the data distribution is a significant imbalance, adopting $wMAPE$ as a performance metric can effectively alleviate zero values issues. In addition, $wMAPE$ allows assigning different weights to different ground truth, thus increasing the evaluation robustness. In addition, MAE and $RMSE$, two widely used metrics in time series forecasting, are adopted to evaluate the models’ performance.

Implementation

All experiments are implemented with Python 3.8.5 and Pytorch 1.12.1 We conduct them on the cloud servers with two NVIDIA Tesla T4 GPUs with 16GB VRAM each. We initialize the network parameters with *Xavier Initialization* [Glorot and Bengio, 2010]. Each parameter is sampled from $N(0, \mu^2)$, where $\mu = -\sqrt{2/(n_{in} + n_{out})}$. n_{in}, n_{out} denote the number of input and output neurons, respectively. In actuality, the λ of ridge regression for solving the koopman matrix in the ITM module is 0.1, the number of child nodes m at the virtual hierarchy is set as 15 during hierarchical sampling. In addition, we train all models by setting the mini-batch size to 256 and using the Adam optimizer with a learning rate of 0.001. Except for MQRNN with the quantile loss at 0.5, all other models choose MSE as the training loss. The number of training epochs is 2 on the dataset, and the value of each experimental result is the average of 5 repeated tests.

5.2 Offline Experiments

Comparison with Baselines

The comparative results are shown in Table 2. For fairness, we compared both the original baseline methods and the im-

Model	Length P	Only label			With CFB as covariate		
		MAE	RMSE	wMAPE	MAE	RMSE	wMAPE
Autoformer	7 days	0.9319	2.9374	0.7030	0.9631	2.9132	0.7265
	14 days	1.0017	2.3737	0.9830	0.9799	2.3566	0.9624
	30 days	0.9658	2.2737	0.9910	1.2101	2.7625	1.2414
Fedformer	7 days	0.9280	2.9147	0.7000	0.9191	2.9100	0.6933
	14 days	0.8744	2.3333	0.8605	0.9071	2.4167	0.8923
	30 days	0.9109	2.1718	0.9347	1.6507	4.7499	1.6933
TFT	7 days	0.9584	2.9184	0.7195	0.9535	2.9043	0.7215
	14 days	0.8643	2.2745	0.8535	0.8524	2.2730	0.8468
	30 days	0.8294	2.3346	0.8494	0.8301	2.2945	0.8693
DLinear	7 days	0.9825	2.9539	0.7412	0.9822	2.9566	0.7410
	14 days	0.8555	2.3279	0.8418	0.8571	2.3572	0.8427
	30 days	0.8125	1.9499	0.8337	0.8089	1.9634	0.8298
Informer	7 days	0.9731	2.9251	0.7341	0.9365	2.9169	0.7065
	14 days	0.8034	2.2653	0.7906	0.8203	2.2969	0.8065
	30 days	0.7699	<u>1.9618</u>	0.7899	0.8063	1.9844	0.8271
iTransformer	7 days	0.9057	2.9261	0.6832	0.9096	2.9086	0.6862
	14 days	0.7755	2.2896	0.7632	0.7891	2.3134	0.7758
	30 days	0.8062	2.0475	0.7694	0.7720	2.0144	0.7364
MQ-RNN	7 days	0.9007	3.0013	0.6895	0.9064	3.0185	0.6830
	14 days	<u>0.7403</u>	2.5217	0.7478	0.7415	2.4554	0.7381
	30 days	<u>0.6958</u>	2.1756	<u>0.7142</u>	0.7029	2.2161	0.7215
Koopa	7 days	0.9024	2.9047	0.6943	<u>0.8927</u>	<u>2.8948</u>	<u>0.6818</u>
	14 days	0.7440	2.3485	0.7326	0.7475	2.4327	0.7350
	30 days	0.7045	2.1943	0.7276	0.6984	2.3456	0.7176
CRAFT	7 days				0.8480	2.8654	0.6706
	14 days				0.7237	2.2696	0.7121
	30 days				0.6895	2.0121	0.7078

Table 2: Comparative results with prediction window length of $P \in \{7, 14, 30\}$ respectively, correspond one-to-one with the look-back window $L \in \{30, 90, 180\}$. The unit of length is days. The best results are highlighted in bold and the second best results are highlighted with a underline.

proved versions with CFB. CRAFT achieves the best performance, significantly outperforming the other baselines. We obtain the following observations from Table 2:

- Compared to the original model, directly integrating CFB into the existing framework does not yield significant performance enhancements. In some cases, it even leads to performance degradation. The experimental results confirm that, despite its indispensable role, effectively applying CFB presents considerable challenges.
- Compared with the optimal baseline, CRAFT improves by at least $\{0.0447, 0.0166, 0.0063\}$ and $\{0.0112, 0.0205, 0.0064\}$ in MAE and $wMAPE$ metrics in the prediction window of $\{7, 14, 30\}$. In $RMSE$ metric, CRAFT ranks the best and the second best when the length of prediction window is 7 and 14. To sum up, CRAFT performs better than baseline models in various prediction lengths, demonstrating stable superiority. The reason behind the excellent results is that CRAFT utilizes the KPM and the ITM module to fully explore the CFB, adopts the ETG to transfer the trend of high-level time series to low-level time series, and employs demand-constrained loss to correct the prediction distribution deviation.
- Experimental results indicate that CRAFT achieves the best results at the prediction length of 7. The reason behind this phenomena is that when the prediction length increases, the sparsity and unknown properties of the CFB become more obvious.
- In the experimental results, the longer the prediction window, the smaller the prediction error. The reason is that the

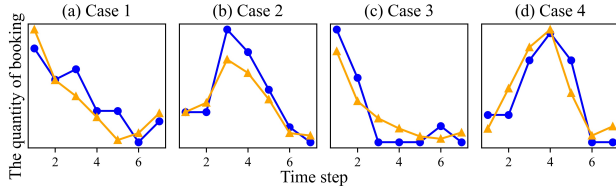


Figure 4: Case study on (a)-(d) four different cases, where blue line is the truth value and the orange line is the prediction of CRAFT.

KPM	ITM	ETG	Demand Loss	MAE	RMSE	wMApe
✓	×	×	×	0.9440	3.1507	0.7122
✓	✓	×	×	0.9090	2.9416	0.6857
✓	✓	✓	×	0.8557	2.7555	0.6455
✓	✓	✓	✓	0.8480	2.7480	0.6397

Table 3: Ablation study of CRAFT.

prediction windows consist of daily data and holiday data, and holiday patterns are more difficult to predict. As the length of the prediction window increases, the proportion of holiday data decreases and the overall prediction error reduces.

Ablation Study

To verify the effectiveness of each module in CRAFT, we conduct an ablation study on the setting of the prediction window’s length is 7, as CRAFT achieves the best results on this condition. The experiment results of the ablation study are listed in Table 3. According to Table 3, we can know that the ITM, ETG module, and the constrain-demand loss all have positive impact on improving the performance of CRAFT. Among them, ITM and ETG module achieve the most obvious improvement with 0.035, 0.053 on *MAE*, 0.2091, 0.1861 on *RMSE*, 0.0265, 0.0402 on *wMAPE*.

Case Study

To verify that the model is effective in capturing future trends, we selected samples from the dataset with different trends for validation. As shown in Figure 4, the trend varies from sample to sample event for the same event impact: some hotels reached their peak in the early stages of the holiday and showed an overall downward trend (Figure 4 (a), (c)); some hotels had high traffic in the middle holiday period and showed an overall mountain shape (Figure 4 (b), (d)). The predicted trend of CRAFT is also not constant but changes with the actual trend of the sample, which indicates the reliability of CRAFT.

In addition, we present the hyperparameter analysis and complexity analysis in Appendix E in our full paper [Zhang *et al.*, 2025].

5.3 Online A/B Test

To further verify the performance of CRAFT in the real online environment, we apply CRAFT to holiday inventory negotiations. In the real application, we need to predict the hotel sales before holidays, and business developers (BD) will check whether the inventory is sufficient based on the prediction results of our model. If not, they will negotiate with the

Holiday	IWR [*]		PHDI [†]	
	MQ-RNN	CRAFT	MQ-RNN	CRAFT
2023 Mid-autumn	0.0513	0.0306	0.3659	0.2983
2023 National Day	0.0534	0.0311	0.3694	0.2990
2024 New Year’s Day	0.0601	0.0354	0.3661	0.3093
2024 Spring Festival	0.0583	0.0337	0.3655	0.3047

^{*} IWR means inventory waste rate. [†] PHDI means the proportion of hotels with depleted inventory.

Table 4: Online A/B test result during holiday.

hotel in advance based on the prediction results to give more inventory. We select the MQ-RNN as the baseline and utilize *IWR* and *PHDI* metrics to measure the overall impact of different models. The definition of *IWR* and *PHDI* refers to Appendix B.4 in our full paper [Zhang *et al.*, 2025]. *IWR* and *PHDI* are defined according to specific scenarios and are the most concerned metrics in BD negotiations. Moreover, as we cannot equally assign daily traffic to each model, such as testing personalized recommendation systems, we randomly divided the hotels into two groups for the MQ-RNN and CRAFT models.

For both the *IWR* and *PHDI* metrics, the smaller the value, the better the model performance. The online A/B test results are shown in Table 4. Compared with MQ-RNN, CRAFT achieves significant improvement on these two metrics. Indeed, based on the data from four holidays, CRAFT method has an average improvement of 0.0231 and an improvement rate of 41.35% on the *IWR* metric. On the *PHDI* metric, the improvement value and improvement rate are 0.0639 and 17.42%, respectively. The results above illustrate the effectiveness of CRAFT in the real application.

6 Conclusion

In this paper, inspired by real-world application, we define **Cross-Future Behavior (CFB)**. CFB is a kind of features that occur before the current time but take effect in the future, containing true information related to future events. For the application of CFB in the TSF, we propose an improved method, named **Cross-Future Behavior Awareness based Time Series Forecasting method (CRAFT)**. CRAFT regards the trend of CFB as prior information to predict the trend of target time series data. We conduct experiments on real-world dataset. Experiments on both offline and online tests demonstrate the effectiveness of CRAFT. However, this paper only conduct experiments on our dataset as the current public available dataset (e.g., ETT [Zhou *et al.*, 2021], ECL¹, Weather²) does not contain the CFB feature or similar feature. In the future, we will further collect related data to form a series benchmark dataset. Moreover, we will continue to generalize the definition of CFB to enable CRAFT method to be applied more broadly.

¹ECL dataset was acquired at <https://archive.ics.uci.edu/ml/datasets/ElectricityLoadDiagrams20112014>.

²Weather dataset was acquired at <https://www.ncei.noaa.gov/data/local-climatological-data/>.

Acknowledgments

This work is supported by Natural Science Foundation of China (No.62302487), AI Dream Project (No.SZSM202402), and Jinan Social and People's Livelihood Major Project (No.202317014).

Contribution Statement

*: Yingwei Zhang and Ke Bu contributed equally to this work and share first authorship. †: Detao Lv is the corresponding author responsible for correspondence.

References

- [Avati *et al.*, 2020] Anand Avati, Tony Duan, Sharon Zhou, Kenneth Jung, Nigam H Shah, and Andrew Y Ng. Count-down regression: sharp and calibrated survival predictions. In *Uncertainty in Artificial Intelligence*, pages 145–155. PMLR, 2020.
- [Bai *et al.*, 1803] Shaojie Bai, J Zico Kolter, and Vladlen Koltun. An empirical evaluation of generic convolutional and recurrent networks for sequence modeling. *arXiv preprint arXiv:1803.01271*, 2(1803):8, 1803.
- [Chen *et al.*, 2020] Yitian Chen, Yanfei Kang, Yixiong Chen, and Zizhuo Wang. Probabilistic forecasting with temporal convolutional neural network. *Neurocomputing*, 399:491–501, 2020.
- [Gao *et al.*, 2022] Chengliang Gao, Fan Zhang, Yue Zhou, Ronggen Feng, Qiang Ru, Kaigui Bian, Renqing He, and Zhizhao Sun. Applying deep learning based probabilistic forecasting to food preparation time for on-demand delivery service. In *Proceedings of the 28th ACM SIGKDD Conference on Knowledge Discovery and Data Mining*, pages 2924–2934, 2022.
- [Glorot and Bengio, 2010] Xavier Glorot and Yoshua Bengio. Understanding the difficulty of training deep feedforward neural networks. In *Proceedings of the thirteenth international conference on artificial intelligence and statistics*, pages 249–256. JMLR Workshop and Conference Proceedings, 2010.
- [Hu *et al.*, 2024] Xuanming Hu, Wei Fan, Haifeng Chen, Pengyang Wang, and Yanjie Fu. Reconstructing missing variables for multivariate time series forecasting via conditional generative flows. In *Proceedings of the 33rd International Joint Conference on Artificial Intelligence (IJCAI)*, Jeju, Korea, 2024.
- [Koopman, 1931] Bernard O Koopman. Hamiltonian systems and transformation in hilbert space. *Proceedings of the National Academy of Sciences*, 17(5):315–318, 1931.
- [Li *et al.*, 2024] Yuxin Li, Wenchao Chen, Xinyue Hu, Bo Chen, Mingyuan Zhou, et al. Transformer-modulated diffusion models for probabilistic multivariate time series forecasting. In *The Twelfth International Conference on Learning Representations*, 2024.
- [Lim *et al.*, 2021] Bryan Lim, Sercan Ö Arık, Nicolas Loeff, and Tomas Pfister. Temporal fusion transformers for interpretable multi-horizon time series forecasting. *International Journal of Forecasting*, 37(4):1748–1764, 2021.
- [Liu *et al.*, 2020] Fan Liu, Xingshe Zhou, Jinli Cao, Zhu Wang, Tianben Wang, Hua Wang, and Yanchun Zhang. Anomaly detection in quasi-periodic time series based on automatic data segmentation and attentional lstm-cnn. *IEEE Transactions on Knowledge and Data Engineering*, 34(6):2626–2640, 2020.
- [Liu *et al.*, 2021] Shizhan Liu, Hang Yu, Cong Liao, Jianguo Li, Weiyao Lin, Alex X Liu, and Schahram Dustdar. Pyraformer: Low-complexity pyramidal attention for long-range time series modeling and forecasting. In *International conference on learning representations*, 2021.
- [Liu *et al.*, 2024a] Yong Liu, Tengge Hu, Haoran Zhang, Haixu Wu, Shiyu Wang, Lintao Ma, and Mingsheng Long. itransformer: Inverted transformers are effective for time series forecasting. In *The Twelfth International Conference on Learning Representations*, 2024.
- [Liu *et al.*, 2024b] Yong Liu, Chenyu Li, Jianmin Wang, and Mingsheng Long. Koopa: Learning non-stationary time series dynamics with koopman predictors. *Advances in Neural Information Processing Systems*, 36, 2024.
- [Lu *et al.*, 2022] Yucheng Lu, Qiang Ji, Liang Wang, Tian-shu Wu, Hongbo Deng, Jian Xu, and Bo Zheng. Stardom: semantic aware deep hierarchical forecasting model for search traffic prediction. In *Proceedings of the 31st ACM International Conference On Information & Knowledge Management*, pages 3352–3360, 2022.
- [Mendis *et al.*, 2024] Kasun Mendis, Manjusri Wickramasinghe, and Pasindu Marasinghe. Multivariate time series forecasting: A review. In *Proceedings of the 2024 2nd Asia Conference on Computer Vision, Image Processing and Pattern Recognition*, pages 1–9, 2024.
- [Mossop and Rahman, 2023] Brandon Mossop and Quazi Abidur Rahman. Infectious disease forecasting using multivariate incomplete time-series: A hybrid architecture with stacked dilated causal convolutions. In *2023 IEEE International Conference on Bioinformatics and Biomedicine (BIBM)*, pages 4220–4227. IEEE, 2023.
- [Nie *et al.*, 2024] Yuqi Nie, Nam H Nguyen, Phanwadee Sinthong, and Jayant Kalagnanam. A time series is worth 64 words: Long-term forecasting with transformers. In *The Eleventh International Conference on Learning Representations*, 2024.
- [Oord *et al.*, 2016] Aaron van den Oord, Sander Dieleman, Heiga Zen, Karen Simonyan, Oriol Vinyals, Alex Graves, Nal Kalchbrenner, Andrew Senior, and Koray Kavukcuoglu. Wavenet: A generative model for raw audio. *arXiv preprint arXiv:1609.03499*, 2016.
- [Rasul *et al.*, 2024] Kashif Rasul, Andrew Bennett, Pablo Vicente, Umang Gupta, Hena Ghonia, Anderson Schneider, and Yuriy Nevmyvaka. Vq-tr: Vector quantized attention for time series forecasting. In *The Twelfth International Conference on Learning Representations*, 2024.

- [Salinas *et al.*, 2020] David Salinas, Valentin Flunkert, Jan Gasthaus, and Tim Januschowski. Deepar: Probabilistic forecasting with autoregressive recurrent networks. *International Journal of Forecasting*, 36(3):1181–1191, 2020.
- [Shetty and Ismail, 2023] Dileep Kumar Shetty and B Ismail. Forecasting stock prices using hybrid non-stationary time series model with ernn. *Communications in Statistics-Simulation and Computation*, 52(3):1026–1040, 2023.
- [Wang *et al.*, 2019] Yuyang Wang, Alex Smola, Danielle Maddix, Jan Gasthaus, Dean Foster, and Tim Januschowski. Deep factors for forecasting. In *International conference on machine learning*, pages 6607–6617. PMLR, 2019.
- [Wang *et al.*, 2024] Xue Wang, Tian Zhou, Qingsong Wen, Jinyang Gao, Bolin Ding, and Rong Jin. Card: Channel aligned robust blend transformer for time series forecasting. In *The Twelfth International Conference on Learning Representations*, 2024.
- [Wen *et al.*, 2017] Ruofeng Wen, Kari Torkkola, Balakrishnan Narayanaswamy, and Dhruv Madeka. A multi-horizon quantile recurrent forecaster. *arXiv preprint arXiv:1711.11053*, 2017.
- [Wen *et al.*, 2023] Qingsong Wen, Tian Zhou, Chaoli Zhang, Weiqi Chen, Ziqing Ma, Junchi Yan, and Liang Sun. Transformers in time series: a survey. In *Proceedings of the Thirty-Second International Joint Conference on Artificial Intelligence*, pages 6778–6786, 2023.
- [Wu *et al.*, 2021] Haixu Wu, Jiehui Xu, Jianmin Wang, and Mingsheng Long. Autoformer: Decomposition transformers with auto-correlation for long-term series forecasting. *Advances in neural information processing systems*, 34:22419–22430, 2021.
- [Yang *et al.*, 2024] Yingnan Yang, Qingling Zhu, and Jianyong Chen. Vcformer: Variable correlation transformer with inherent lagged correlation for multivariate time series forecasting. *Proceedings of the 33rd International Joint Conference on Artificial Intelligence (IJCAI)*, Jeju, Korea, 2024.
- [Yin *et al.*, 2022] Changchang Yin, Sayoko E Moroi, and Ping Zhang. Predicting age-related macular degeneration progression with contrastive attention and time-aware lstm. In *Proceedings of the 28th ACM SIGKDD Conference on Knowledge Discovery and Data Mining*, pages 4402–4412, 2022.
- [Zeng *et al.*, 2023] Ailing Zeng, Muxi Chen, Lei Zhang, and Qiang Xu. Are transformers effective for time series forecasting? In *Proceedings of the AAAI conference on artificial intelligence*, volume 37, pages 11121–11128, 2023.
- [Zhang *et al.*, 2025] Yingwei Zhang, Ke Bu, Zhuoran Zhuang, Tao Xie, Yao Yu, Dong Li, Yang Guo, and Detao Lv. Craft: Time series forecasting with cross-future behavior awareness, 2025.
- [Zhao and Shen, 2024] Lifan Zhao and Yanyan Shen. Rethinking channel dependence for multivariate time series forecasting: Learning from leading indicators. In *The Twelfth International Conference on Learning Representations*, 2024.
- [Zhou *et al.*, 2021] Haoyi Zhou, Shanghang Zhang, Jieqi Peng, Shuai Zhang, Jianxin Li, Hui Xiong, and Wancai Zhang. Informer: Beyond efficient transformer for long sequence time-series forecasting. In *Proceedings of the AAAI conference on artificial intelligence*, volume 35, pages 11106–11115, 2021.
- [Zhou *et al.*, 2022] Tian Zhou, Ziqing Ma, Qingsong Wen, Xue Wang, Liang Sun, and Rong Jin. Fedformer: Frequency enhanced decomposed transformer for long-term series forecasting. In *International conference on machine learning*, pages 27268–27286. PMLR, 2022.
- [Zhu *et al.*, 2023] Ruitao Zhu, Detao Lv, Yao Yu, Ruihao Zhu, Zhenzhe Zheng, Ke Bu, Quan Lu, and Fan Wu. Linet: A location and intention-aware neural network for hotel group recommendation. In *Proceedings of the ACM Web Conference 2023*, pages 779–789, 2023.
- [Zonghan *et al.*, 2019] Wu Zonghan, Pan Shirui, Long Guodong, Jiang Jing, and Zhang Chengqi. Graph wavenet for deep spatial-temporal graph modeling. In *Proceedings of the Twenty-Eighth International Joint Conference on Artificial Intelligence, IJCAI 2019, Macao, China, August 10-16, 2019*, pages 1907–1913, 2019.